CH-99-6-1 (4265) (RP-949)

Measurements and Computations of Room Airflow with Displacement Ventilation

Xiaoxiong Yuan, Ph.D.

Qingyan Chen, Ph.D.
Member ASHRAE

Leon R. Glicksman, Ph.D.
Member ASHRAE

Yongqing Hu

Xudong Yang
Student Member ASHRAE

ABSTRACT

This paper presents a set of detailed experimental data of room airflow with displacement ventilation. These data were obtained from a new environmental test facility. The measurements were conducted for three typical room configurations: a small office, a large office with partitions, and a classroom.

The distributions of air velocity, air velocity fluctuation, and air temperature were measured by omnidirectional hot-sphere anemometers, and contaminant concentrations were measured by tracer gas at 54 points in the rooms. Smoke was used to observe airflow. The data also include the wall surface temperature distribution, air supply parameters, and the age of air at several locations in the rooms.

A computational fluid dynamics (CFD) program with the Re-Normalization Group (RNG) k-ε model was also used to predict the indoor airflow. The agreement between the computed results and measured data of air temperature and velocity is good. However, some discrepancies exist in the computed and measured concentrations and velocity fluctuation.

INTRODUCTION

Displacement ventilation may provide better indoor air quality than mixing ventilation and also save energy, but there is a question of the usefulness of this technology in U.S. buildings with their higher cooling requirements. A first step in preparing a design guideline for displacement ventilation is careful experiments in several different buildings.

Two main approaches are available for the study of airflow and pollutant transport in buildings: experimental investigation and computer simulation. In principle, direct measurements give the most realistic information concerning indoor airflow and pollutant transport, such as the distributions of air velocity, temperature, relative humidity, and contaminant concentrations. Because the measurements must be made at many locations, direct measurements of the distributions are very expensive and time consuming. A complete measurement may take many months of work. Moreover, to obtain conclusive results, the airflow and temperature from the heating, ventilating, and air-conditioning (HVAC) systems and the temperatures of the building enclosure should be maintained unchanged during the experiment. This is especially difficult because outdoor conditions change over time and the temperatures of the building enclosure and the airflow and temperature from the HVAC systems will also change accordingly.

An environmental chamber may be used to simulate an indoor space, to isolate the measured system from the external world. However, such an environmental chamber costs more than $300,000 with necessary equipment for measuring air velocity, temperature, relative humidity, and contaminant concentrations. Furthermore, it may not be easy to change from one spatial configuration to another.

On the other hand, the airflow and pollutant transport can be determined computationally by solving a set of conservation equations describing the flow, energy, and contaminants in the system. Due to the limitations of the experimental approach and the increase in performance and affordability of high-speed computers, the numerical solution of these conservation equations provides a practical option for computing the airflow and pollutant distributions in buildings. The method is the computational fluid dynamics (CFD) technique.

The CFD technique is a powerful tool for obtaining information about the indoor environment, such as airflow pattern

Xiaoxiong Yuan was a post-doctoral associate (he is currently a senior engineer at Applied Materials, Inc., Santa Clara, Calif.) **Qingyan (Yan) Chen** is an associate professor, **Leon R. Glicksman** is a professor, **Yongqing Hu** is a research technician, and **Xudong Yang** is a research assistant in the Department of Architecture, Massachusetts Institute of Technology, Cambridge.

and the distributions of air velocity, temperature, turbulence intensity, and contaminant concentrations. Due to limited computer power and capacity available at present, turbulence models have to be used with the CFD technique in order to solve flow motion. The use of turbulence models leads to uncertainties in the computed results because the models are not universal. Therefore, it is essential to validate a CFD program by experimental data.

Many experimental data are available in the literature, but very few of them can be used for validation. Experimental data for CFD validation must contain detailed information about flow and thermal boundary conditions as well as flow and thermal parameters measured in the space. The data must also include an error analysis. Unfortunately, not many of the experimental data include such detailed information. Popular data for validating room airflow are from Cheesewright et al. (1986) and Nielsen et al. (1978). Cheesewright's data are for natural convection and Nielsen's for forced convection. However, it is still not certain that a CFD program validated by their data can be used for normal room airflow with mixed convection (a combination of natural and forced convection).

This paper presents detailed experimental data for displacement ventilation. Displacement ventilation is mixed convection and represents ventilation reality in many buildings. If a CFD program is validated by experimental data for displacement ventilation, the program should be able to predict other indoor environments. The flow characteristics of displacement ventilation and other mixing ventilation are similar—both have strong pressure and buoyancy-driven flows.

The data presented in this paper will be used to validate a CFD program with a suitable turbulence model. There are many turbulence models available. The "standard" k-ε model (Launder and Spalding 1974) is probably most widely used in engineering calculations due to its relative simplicity. However, the model sometimes provides poor results for indoor airflow. Many modifications have been applied to the standard model. However, the modified models do not have general applicability for indoor airflow. Chen (1995, 1996) calculated the various indoor flows with eight different turbulence models. His study concluded that the Re-Normalization Group (RNG) k-ε model (Yokhot et al. 1992) is the best among the eddy-viscosity models tested. This paper will also compare this model's prediction for displacement ventilation in a room with the experimental data.

EXPERIMENTAL FACILITY

The Chambers and HVAC Systems

The environmental test facility built to be used for ASHRAE Research Project 949 is also used for research and the teaching of indoor air quality, thermal comfort, energy efficiency, thermal insulation, and HVAC systems.

The test facility, shown in Figure 1, consists of a well-insulated enclosure. Not shown in the figure are two doors at either end. A movable wall divides the enclosure into a test chamber and a climate chamber. At present, the larger one is used as the test chamber and the smaller one as the climate chamber. The lower part of the movable wall is an insulated exterior wall, and the upper part is a double-glazed window extending almost the whole width. Table 1 shows the dimensions and thermal resistance of the chambers.

The test chamber has two linear diffusers, two circular ceiling diffusers, a grille ceiling exhaust, two flexible

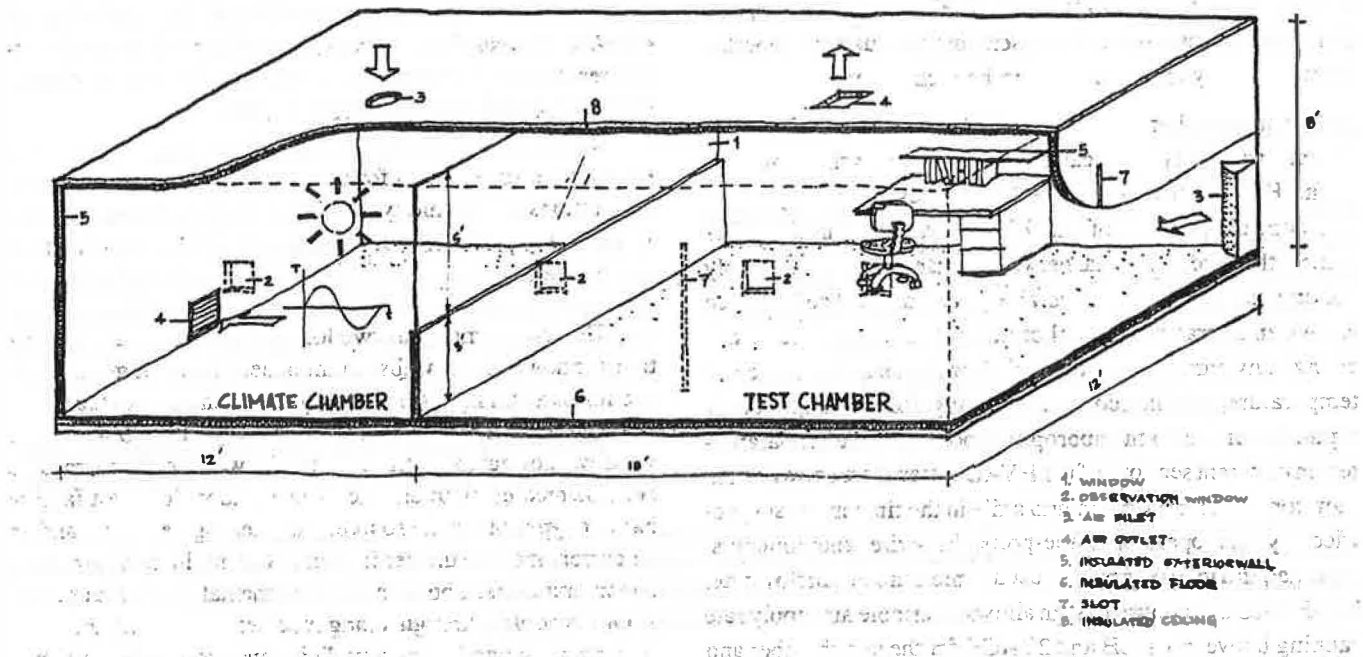

Figure 1 Sketch of the test facility.

TABLE 1
Dimensions, Thermal Resistance, and HVAC System Capacities of the Test Facility

		Test Chamber	Climate Chamber
Dimensions	Length	17 ft (5.16 m)	10 ft (3.08 m)
	Width	12 ft (3.65 m)	
	Height	8 ft (2.43 m)	
	Partition height	3.9 ft (1.16 m)	
	Window width	11.5 ft (3.45 m)	
Thermal Resistance	Partition wall	30 $ft^2 \cdot h \cdot °F/Btu$ (5.3 $K \cdot m^2/W$)	
	Partition window	1.5 $ft^2 \cdot h \cdot °F/Btu$ (0.27 $K \cdot m^2/W$)	
	Other walls	30 $ft^2 \cdot h \cdot °F/Btu$ (5.3 $K \cdot m^2/W$)	
	Ceiling	30 $ft^2 \cdot h \cdot °F/Btu$ (5.3 $K \cdot m^2/W$)	
	Floor	30 $ft^2 \cdot h \cdot °F/Btu$ (5.3 $K \cdot m^2/W$)	
	Door	30 $ft^2 \cdot h \cdot °F/Btu$ (5.3 $K \cdot m^2/W$)	
Capacities of HVAC System	Preheater	8 kW	
	Supply fan	560 cfm (930 m^3/h)	
	Chiller	21 kW	Share with the test chamber
	Reheater	8 kW	
	Humidifier	11 kg-steam/h	None
	Return fan	560 cfm (930 m^3/h)	
	Dampers	560 cfm (930 m^3/h)	

displacement diffusers, a grille diffuser installed on the rear wall near the ceiling, and another grille exhaust on the rear wall near the floor. The climate chamber has one ceiling diffuser, one rear wall diffuser, one ceiling exhaust, and one rear wall exhaust. All the diffusers and exhausts can operate simultaneously or individually in both chambers.

Each chamber has a separate HVAC system. The two systems are nearly identical. Table 1 also shows the capacities of the HVAC systems. Figure 2 illustrates the configuration and control interface of the HVAC system. Three louvers control the outdoor air rate between 0% and 100%. The supply fan and return fan have a variable-speed drive. The interface allows an interactive control of the systems. An operator can change any parameter, such as airflow rate, supply and return temperature, and humidity, by moving the ▶ signs or by typing a number to the appropriate position. The air parameters in different sections of the HVAC systems are shown in the monitor and/or are written into a file in the time interval specified by the operator. Nine-probe hot-wire anemometers, arranged in a matrix form, are used to measure the airflow rate. The HVAC and control design allows a variable air supply rate ranging between 1 ACH and 20 ACH for the test chamber and 2 ACH to 40 ACH for the climate chamber.

Equipment

The major measuring equipment of the test facility includes:

- A flow visualization system for observing airflow patterns
- A hot-sphere anemometer system for air velocity, velocity fluctuation, and temperature measurements
- A tracer-gas system for measuring contaminant concentrations and humidity
- A thermocouple system for measuring surface and air temperatures

The test chamber has two long slots and several observation windows on the walls. Light penetrates through the slots and forms a thin light sheet. By injecting smoke into the room, the airflow pattern can be observed through those observation windows normal to the light sheet. The walls of the room have been painted black to enhance visualization. The test facility has two types of smoke source: a theater fog generator and an air current kit. The theater fog generator produces smoke with a temperature far above the environmental temperature. The smoke is cooled through a long tube before entering the room to approach neutral buoyancy. This generator produces a large amount of smoke and is good for observing how supply air is

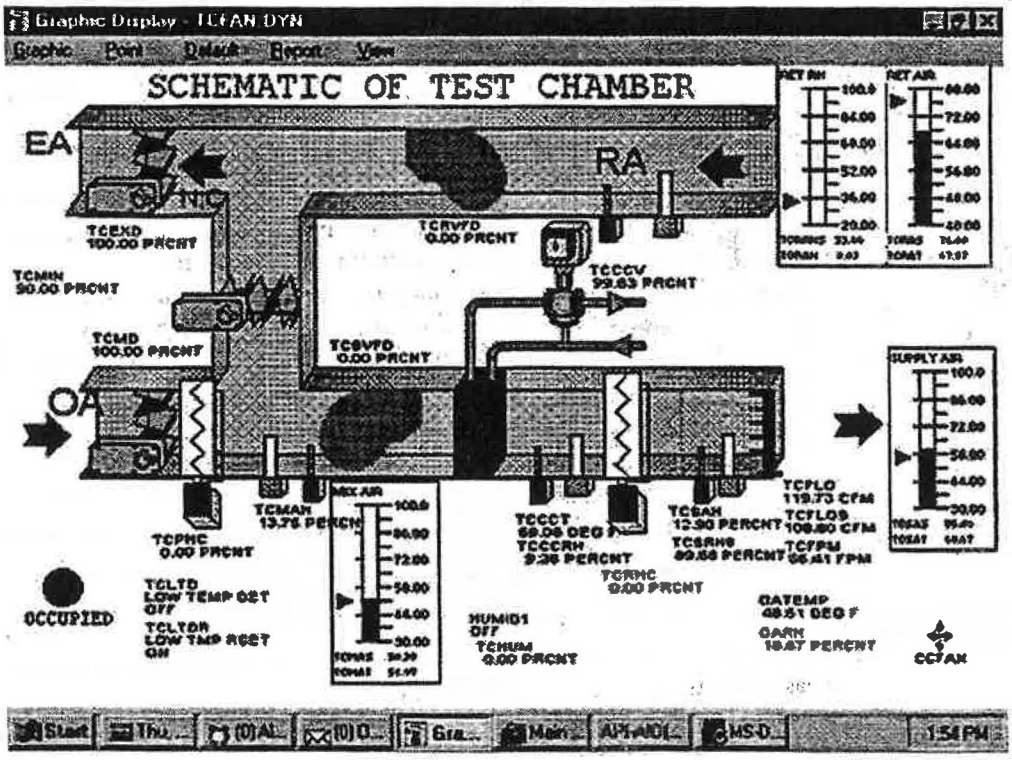

Figure 2 The control interface of the HVAC system.

distributed in the room. However, it is not ideal for visualizing the airflow pattern in a particular area. The air current kit remedies this problem. The kit generates a very small amount of smoke locally.

Air velocity in the occupied zone is often lower than 50 fpm (0.25 m/s) because of the comfort requirements. Most hot-sphere and hot-wire anemometers have great uncertainties when they are used for the measurement of low velocities. The reason is that the natural convection from the hot sphere or hot wire produces a false air velocity of the same magnitude. Although a laser doppler anemometer (LDA) can be used, the time and effort are tremendous because the measurements must be done for many locations in a room and it is difficult to move the LDA to different measuring locations. In recent years, particle image velocimetric (PIV) systems have attracted considerable attention. A PIV system can measure two-dimensional field velocities. However, at present, a PIV system is not able to measure an area larger than 2 ft × 2 ft (0.5 m × 0.5 m) with a reasonable resolution, even with a powerful Nd-Yag laser and a good recorder. It is not feasible to use the PIV system for the field measurements in an indoor space nowadays.

Hence, there is no effective technique to measure low air velocities throughout an indoor space. In the experiment, we used the hot-sphere anemometers for the measurements of air velocity, velocity fluctuation, and temperature in the room. An analog/digital data (ADD) board was used for data acquisition. For velocity, the measurement range of the hot-sphere anemometers is 10 fpm to 1000 fpm (0.05 m/s to 5 m/s); the repeatability is 2 fpm (0.01 m/s), or 2% of the readings. The anemometers cannot reliably measure velocity when the magnitude is lower than 20 fpm (0.10 m/s) The measuring errors for air temperature are 0.5°F (0.3 K), including the errors introduced by the data acquisition systems. Since the probe size is large (about 1/8 in. or 0.003 m in diameter), the probes are not sensitive to high-frequency velocity fluctuation, and it is difficult to estimate the errors for velocity fluctuation.

A multi-gas monitor and analyzer system is used to determine indoor air quality. The tracer-gas system can measure many different types of tracer gases. The present investigation used SF_6 and CO_2. SF_6 is better than CO_2 because the background concentration of SF_6 is almost zero. CO_2 is inexpensive and was used to check the results obtained with SF_6. In addition, the water vapor concentration was also measured to determine relative humidity in the room. The error for measuring concentration is at an acceptable 10%.

Thermocouples were used to measure air temperature and surface temperature of the room enclosures. Many state-of-the-art data acquisition systems use ADD boards. However, most ADD boards we tested have a 0.9°F (0.4 K) error and have at least 0.4°F/ month (0.2 K/month) drift. Therefore, we decided to use a data logger and found that the error for measuring temperature by the entire system is about 0.8°F (0.4 K).

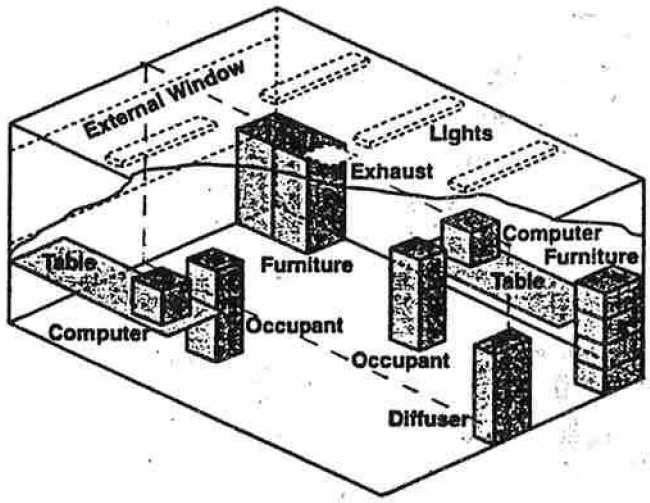

Figure 3 *Space layout of a two-person office used in the experiment.*

Test Procedure

We conducted several measurements with different configurations: a small office, a large office with partitions, and a classroom. Figure 3 shows the two-person small office configuration used in the experiment.

A perforated displacement diffuser, 1.7 ft (0.5 m) wide and 3.6 ft (1.1 m) high, was placed at the middle of the right-side wall near the floor. The effective area ratio is 10%. The exhaust, 1.4 ft × 1.4 ft (0.43 m × 0.43 m), was at the center of the ceiling.

The occupants in the test room were simulated by two boxes, 1.3 ft (0.4 m) long, 1.2 ft (0.35 m) wide, and 3.6 ft (1.1 m) high, each heated by three 25 W lightbulbs. The measured surface temperature was between 82°F and 86°F (28°C and 30°C). Two point sources of SF_6 were introduced at the top of the two boxes to simulate contaminants from the occupants, with an initial velocity of 9 fpm (0.045 m/s) in the horizontal direction. Two PCs were used to generate heat. One generated 108 W and the other 173 W. Six 34 W fluorescent lamps were used during the experiment as overhead lighting. In addition, two tables and two file cabinets were also in the room. The ventilation rate was 4 ACH, corresponding to a face velocity of 18 fpm (0.09 m/s) at the diffuser. The supply air temperature was controlled at 62.5°F (17.0°C). The window surface temperature was 81.1°F - 82.6°F (27.3°C - 28.1°C), and the surface temperature on the movable wall was 75.6°F - 9.9°F (24.2°C - 26.6°C). The surface temperatures on the other walls were 73.9°F - 78.8°F (23.3°C - 26.0°C).

Five movable poles were placed in the test room, each supporting six hot-sphere anemometers and six air-sampling tubes. Additionally, two thermocouples were attached on each pole to measure air temperature near the floor and ceiling. A total of 40 thermocouples were used to measure the surface temperatures of the floor, ceiling, window, and walls.

Measurements were conducted under steady-state conditions by stabilizing the room thermal and fluid conditions for more than 12 hours before recording the data. Air velocity, air temperature, and SF_6 concentration were measured at nine different positions with a total of 54 measuring points for air velocity, 72 for air temperature, and 54 for tracer gas.

The measured air velocities can be used for determining turbulence intensity, and the measured concentrations can be used to find the local mean age of air. Since the omnidirectional anemometers have a large uncertainty in measuring low air velocity, we feel the fluctuating velocity, $|u'|$, could provide more accurate information than turbulence intensity. This investigation has further used the step-up and decay method to determine the age of air, τ:

$$\tau = \int_0^\infty \left[1 - \frac{c(t) - c(0)}{c(\infty) - c(0)}\right] dt \quad \text{(step-up)}, \tag{1}$$

$$\tau = \frac{\int_0^\infty [c(t) - c(\infty)]\,dt}{c(0) - c(\infty)} \quad \text{(decay)}, \tag{2}$$

where $c(t)$, $c(0)$, and $c(\infty)$ are the tracer-gas concentration measured at time = t, 0, and infinite, respectively.

THE COMPUTATIONAL FLUID DYNAMICS MODEL

The Re-Normalization Group (RNG) k-ε Model

The governing equations for the RNG k-ε model are as follows.

$$\frac{\partial}{\partial t}(\rho\phi) + \frac{\partial}{\partial x_j}(\rho u_j \phi) = \frac{\partial}{\partial x_j}\left(\Gamma_\phi \frac{\partial \phi}{\partial x_j}\right) + S_\phi \tag{3}$$

where

t = time
ρ = air density, kg/m^3
ϕ = 1 for mass continuity
= u_j (j = 1, 2, and 3) for three components of momentum
= k for kinetic energy of turbulence
= ε for dissipation rate of turbulence energy
= T for temperature
= c for contaminant concentration
x_j = coordinate
$\Gamma_{\phi,eff}$ = effective diffusion coefficient
S_ϕ = source term

The ϕ, Γ_ϕ, and S_ϕ are further listed in Table 2.

Boundary Conditions

Since the RNG k-ε model is valid for high Reynolds number turbulent flow, wall functions are needed for the near wall region where the flow Reynolds number is low. The present investigation uses the following wall functions (Launder and Spalding 1974):

TABLE 2
Values of ϕ, Γ_ϕ, and S_ϕ

ϕ	Γ_ϕ	S_ϕ
1	0	0
u_i	$\mu + \mu_t$	
k	$(\mu + \mu_t)/\sigma_k$	$G - \rho\varepsilon + G_B$
ε	$(\mu + \mu_t)/\sigma_\varepsilon$	$(C_{\varepsilon 1} G - C_{\varepsilon 2}\rho\varepsilon + C_{\varepsilon 3} G_B)\varepsilon/k + R$
T	$\mu/\sigma_l + \mu_t/\sigma_t$	S_T
C	$(\mu + \mu_t)/\sigma_c$	S_c

where

μ is laminar viscosity

$\mu_t = \rho C_\mu \frac{k^2}{\varepsilon}$ is turbulent viscosity

$G = \mu_t \frac{\partial u_i}{\partial x_j}\left(\frac{\partial u_i}{\partial x_j} + \frac{\partial u_j}{\partial x_i}\right)$ is the turbulent production

$G_B = -g_i \beta \frac{\mu_t}{Pr_t}\frac{\partial T}{\partial x_i}$ is the turbulent production due to buoyancy

$R = \frac{C_\mu \eta^3 (1 - \eta/\eta_0)\varepsilon^2}{1 + \beta\eta^3}\frac{1}{k}$ is the source term from renormalization

$\eta = S\frac{k}{\varepsilon}$, $S = (2S_{ij}S_{ij})^{1/2}$, $S_{ij} = \frac{1}{2}\left(\frac{\partial u_i}{\partial x_j} + \frac{\partial u_j}{\partial x_i}\right)$

$C_\mu = 0.0845$, $C_{\varepsilon 1} = 1.42$, $C_{\varepsilon 2} = 1.68$, $C_{\varepsilon 3} = 1.0$ are the model constants

$\sigma_k = 0.7194$, $\sigma_\varepsilon = 0.7194$, $\sigma_l = 0.71$, $\sigma_t = 0.9$, $\sigma_c = 1.0$ are Prandtl or Schmidt numbers

For velocity:

$$U = \left(\frac{\tau}{\rho}\right)^{1/2}\frac{1}{\kappa}\log\left(\frac{y}{y^*}E\right) \quad (4)$$

where

U = velocity parallel to the wall
τ = wall shear stress
κ = von Karman constant (0.41)
y = distance between the first grid node and the wall
E = an integration constant (9.0)
y^* = a length scale

For kinetic energy of turbulence:

$$k = \frac{1}{C_\mu^{1/2}}\left(\frac{\tau}{\rho}\right) \quad (5)$$

For dissipation rate of turbulent kinetic energy:

$$\varepsilon = \left(\frac{\tau}{\rho}\right)^{3/2}\frac{1}{\kappa y} \quad (6)$$

For temperature:

$$q = h_c(T_w - T) \quad (7)$$

where

q = heat flux
h_c = convective heat transfer coefficient
T_w = wall temperature

We use Equation 7 for temperature boundary instead of the "standard" wall function proposed by Launder and Spalding (1974) because the wall function would predict grid-dependent heat flux and cause an unacceptable error. The h_c used is based on our experimental data (Chen et al. 1989). This is undesirable in numerical prediction because the h_c is generally unknown. Very recently, we developed a new one-equation model for the near wall flow (Xu 1998). The heat transfer can be correctly calculated with the new model.

Numerical Technique

The governing equations are solved numerically. The whole computational domain, the space of the room, needs to be divided into a number of finite volumes by a grid system. The flow variables, such as velocity, temperature, and concen-

TABLE 3
Grid Refinement

Grid Size	CPU Time (Hour)
72 × 66 × 36	180
48 × 44 × 24	45
29 × 30 × 19	13

tration, are solved at the center of each finite volume. The more grids used, the more accurate the results will be. However, a fine grid will cost more computing time and capacity. Table 3 shows the computing time for three different grid sizes. The difference between the results with two finer grids is very small; therefore, we use a 48 × 44 × 24 grid for comparison with the experimental data.

A commercial CFD code was used for the computations. By default, the code uses the finite-volume method and the upwind-difference-scheme for the convection term. The convergence criterion was set such that the respective sums of the absolute residuals of sources of p, u_i, T, c, k, and ε must be less than 10^{-3}.

RESULTS

Figure 4 shows the flow pattern, observed by using smoke and computed by the CFD technique, in the midsection through the diffuser (the dashed line in Figure 3). The velocity determined from the smoke visualization is rather reliable because the speed is low. The computed flow pattern agrees with the observed one. Due to buoyancy, the cold air from the supply diffuser spreads at the floor level. This cold airflow is like a jet and induces the surrounding air. As a result, the induction causes a reverse flow in the layer between 1.5 ft to 3 ft (0.5 m to 1 m) above the floor. The figure does not show the thermal plumes generated by occupants and computers because they are in a different section.

Figures 5 through 8 present, respectively, the measured and computed temperature, SF_6 concentration, velocity, and velocity fluctuation in the office. The measurements were done with nine poles; each pole had ten sensors to measure temperature and six sensors to measure velocity and tracer-gas concentration. The vertical axes are dimensionless elevation normalized by room height ($Z = 0$ is the floor and $Z = 1$ is the ceiling). The horizontal axes are dimensionless measured parameters.

Figure 5 clearly shows that the displacement ventilation system created temperature stratification. The temperature gradient in the lower part of the office is much larger than the one in the upper part because most heat sources (occupants and computers) are located in the lower part of the room and airflow changes direction in the lower part. Since occupants stay in the lower part of the room, the temperature stratification represents a potential risk of draft. One important criterion in the design of a displacement ventilation system is to ensure that the temperature difference is sufficiently small between the head and foot level. The agreement between the computed temperature and measured data is excellent.

Figure 6 shows the tracer-gas concentration profiles in the room. The tracer-gas sources were introduced at the head level of the two occupants (the two small squares in the right bottom figure). The SF_6 concentration in the occupied zone is much lower than in the upper zone. The concentration increases rapidly between Z of 0.4 and 0.5, which can be considered as the stratification height. Since convective flow around the human body may bring the air at the lower level to the breathing level, displacement ventilation provides better indoor air quality than mixing ventilation.

There are discrepancies between the computed concentration profile and the measured data. Since the tracer gas is a point source and recirculating flow exists in the upper part of the office, the tracer-gas concentration in the upper part is not uniform and very sensitive to the position and boundary conditions. For example, the results for pole 9 show a difference in the concentration distributions between two positions that are only 1 ft (0.3 m) apart. Nevertheless, the accuracy of the computation is acceptable.

Figure 7 shows that the velocity in most of the space, except near the floor, is lower than 10 fpm (0.05 m/s). The

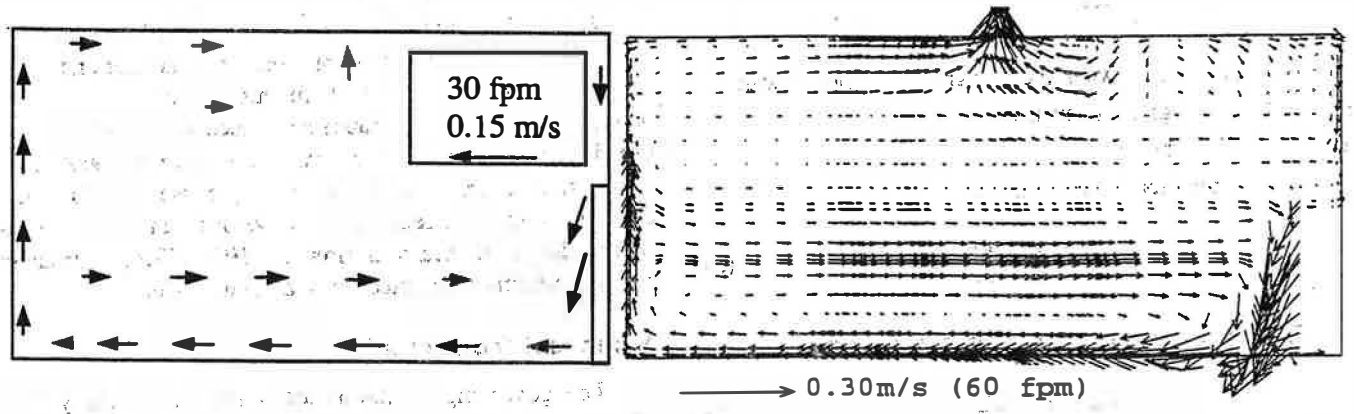

Figure 4 The airflow pattern observed by using smoke visualization and computed by the CFD program (side view of the room). The length of the arrow is proportional to the velocity level.

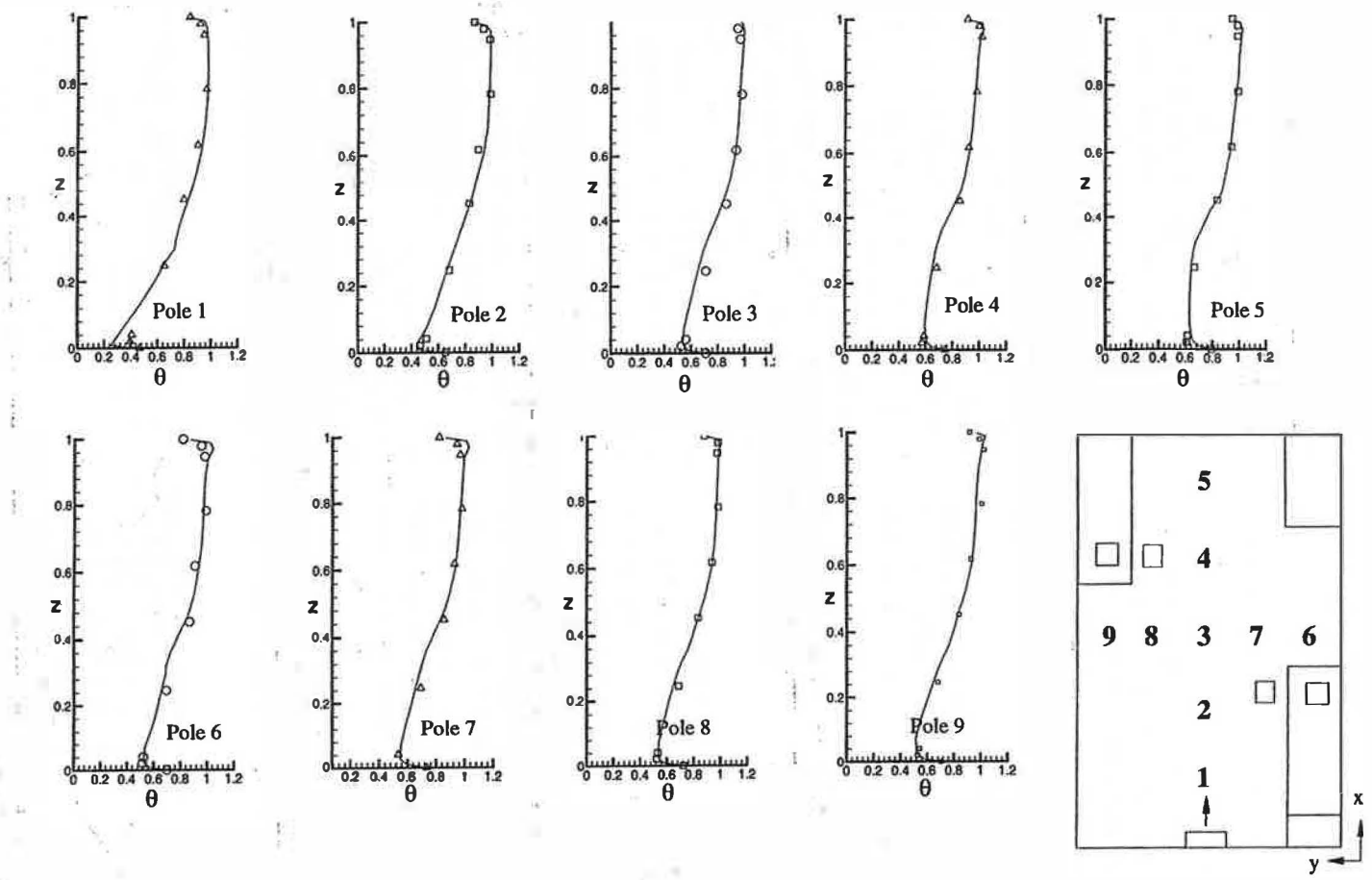

Figure 5 *Comparison of the vertical temperature profiles for a small office.* $\theta = (T - T_s)/(T_e - T_s)$, $T_s = 62.6°F$ *(17.0°C),* $T_e = 80.1°F$ *(26.7°C),* $Z = z/h$, $h = 8$ *ft (2.43 m). Symbols: measurement, Lines: computation.*

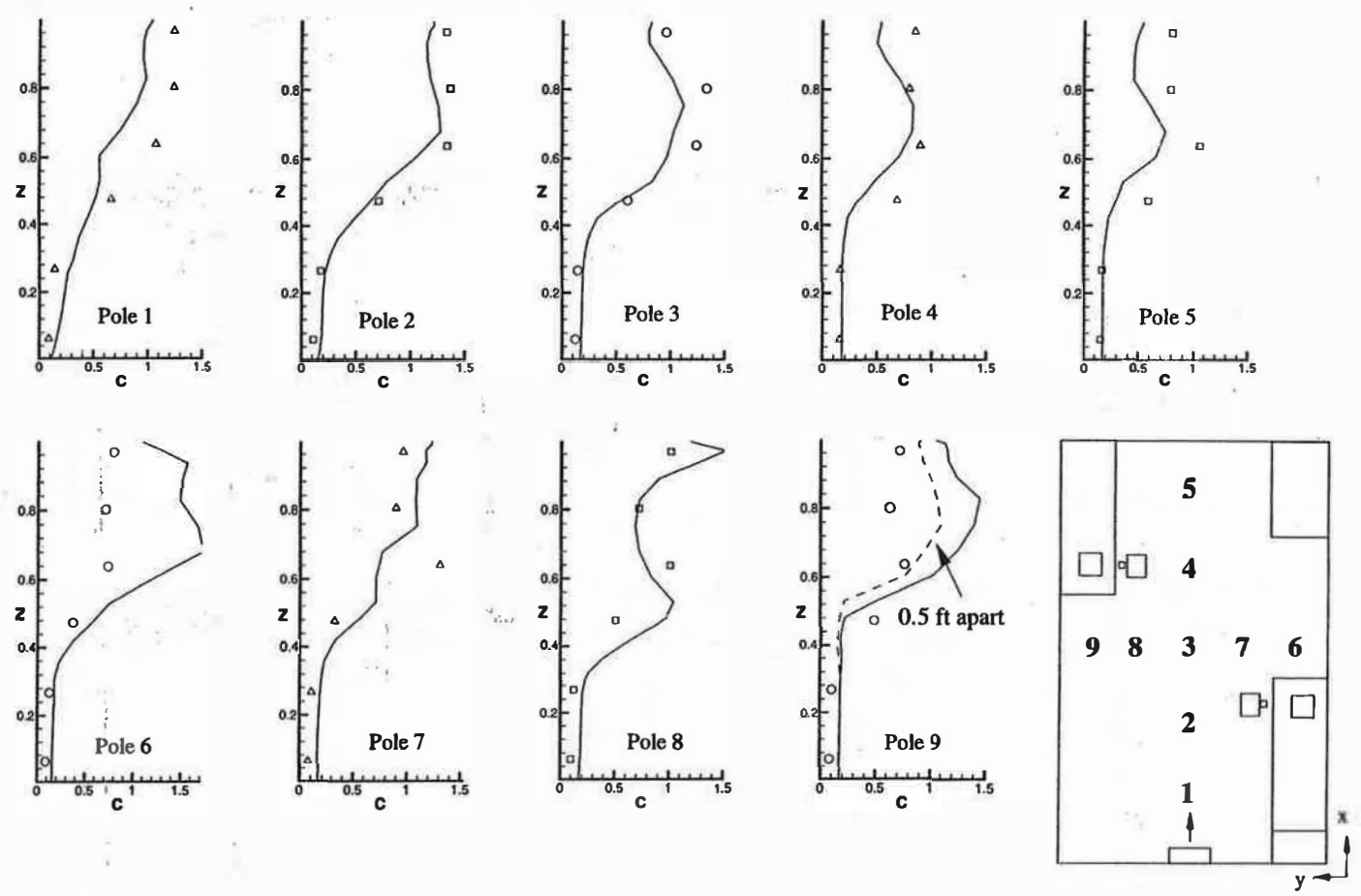

Figure 6 *Comparison of the concentration of SF_6 for a small office.* $C = (c - c_s)/(c_e - c_s)$, $c_s = 0$ *ppm*, $c_e = 0.42$ *ppm*, $Z = z/h$, $h =$ *8 ft (2.43 m). Symbols: measurement, Lines: computation.*

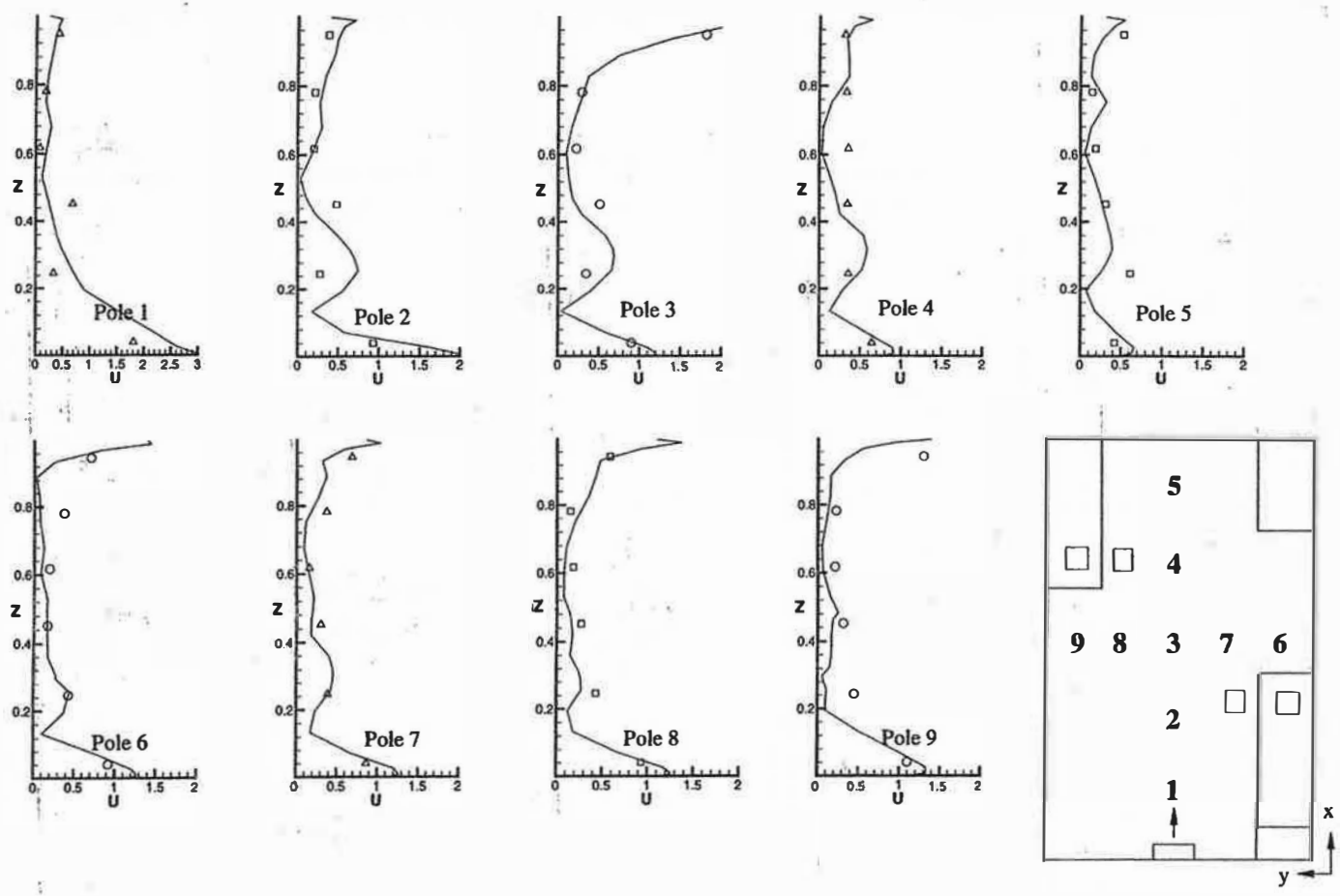

Figure 7 *Comparison of the velocity profiles for a small office.* $U = u/u_s$, u_s = *18 fpm (0.09 m/s),* $Z = z/h$, h = *8 ft (2.43 m). Symbols: measurement, Lines: computation.*

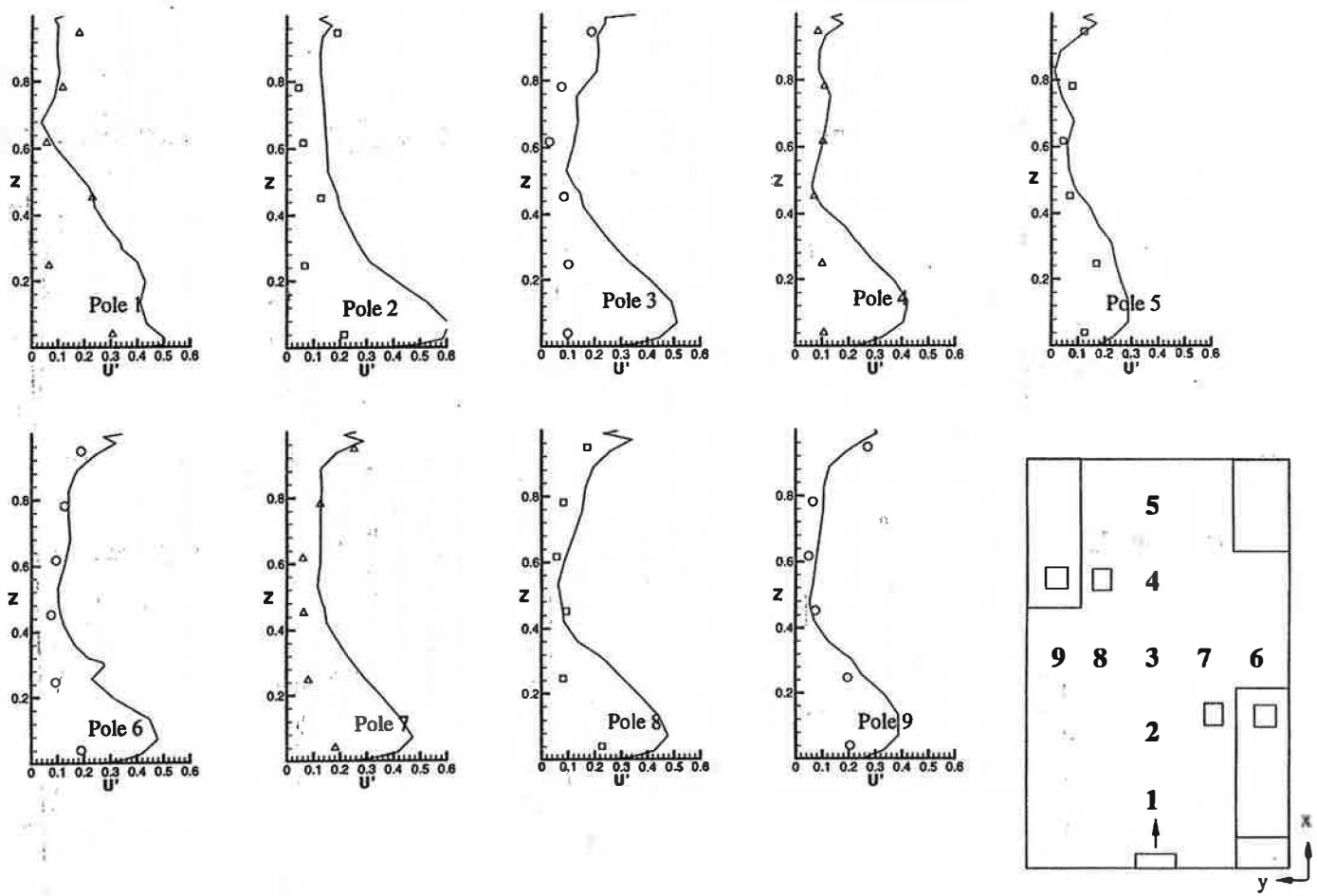

Figure 8 *Comparison of the fluctuating velocity for a small office.* U' = u'/u_s, u_s = *18 fpm (0.09 m/s),* Z = z/h, h = *8 ft (2.43 m). Symbols: measurement, Lines: computation.*

magnitude is so low that the hot-sphere anemometers may fail to give accurate results, but the computed results agree with the data. The measured velocity is also close to that observed through the use of smoke. The velocity near the floor is larger than that in the center of the room because the diffuser is installed at floor level. Draft risk exists in the near diffuser area, such as that indicated in pole 1, where the air velocity is high and the air temperature is low.

The experiment also measured velocity fluctuation. Figure 8 shows the normalized fluctuating velocity by the mean supply air velocity, instead of the local mean velocity, in order to avoid additional uncertainty of the low local mean velocity. The computed profiles in the figure are the quantities of $\sqrt{2k}$, where k is the turbulent kinetic energy. The computed values are larger than the measured ones, which might be due to the errors introduced by the anemometers we used for measurement of the fluctuating velocity. Because of the large probe size, 1/8 in. (3 mm) in diameter, the anemometers may not be able to measure the high-frequency velocity fluctuations. Furthermore, the turbulence model may not accurately calculate turbulent energy. Therefore, it is not surprising to see the large discrepancies between the computed profiles and measured data.

Figure 9 shows the measured transient CO_2 concentration at the middle of pole 4. From the measured data, we have calculated the age of air in the office. Figure 10 compares the computed (contours) and measured (values in boxes) age of air in the midsection of the office. Table 4 further shows that the measured age of air is 10% smaller than the computed one. The age of air is younger in the lower part of the office with displacement ventilation than in the upper part. This is why displacement ventilation can provide better indoor air quality in the occupied zone, that is, in the lower part of the space.

Due to limited space available in this paper, the results presented here are not complete. We have prepared a separate report that details all the measured data and thermal and fluid boundary conditions for the small office, a large office with partitions, and a classroom. The report is available on-line.

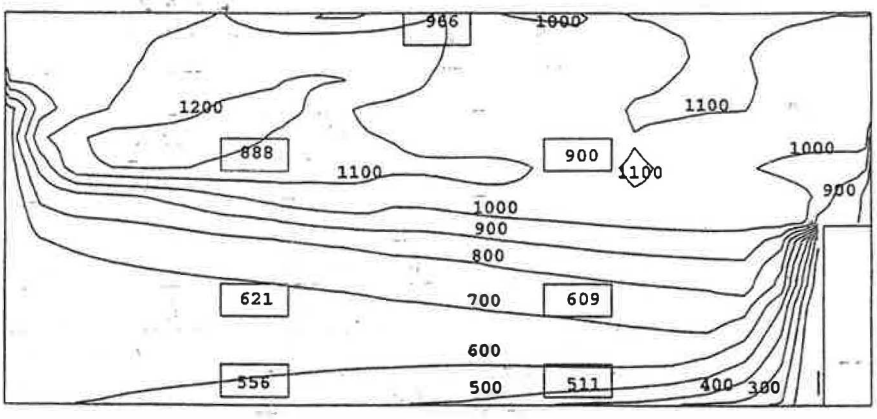

Figure 10 The computed (contours) and measured (values in boxes) age of air in the midsection of the office.

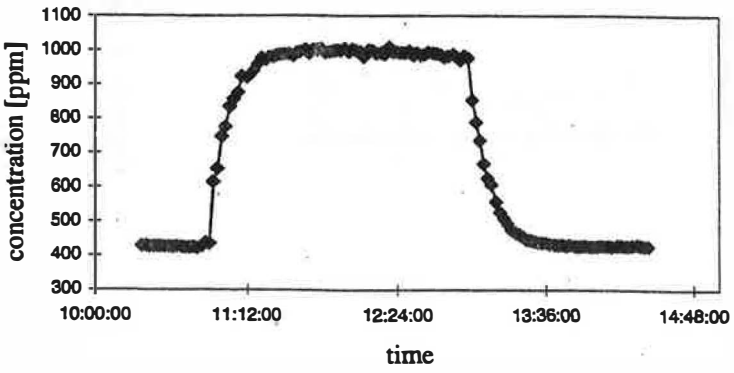

Figure 9 Transient CO_2 concentration profile for determining the age of air.

CONCLUSIONS

Experimental data of displacement ventilation for a small office, a large office with partitions, and a classroom are available for validation of CFD programs. The data include detailed information, such as

- thermal and flow boundary conditions;
- airflow patterns observed by using smoke;
- the distributions of air temperature, concentration of tracer gas, air velocity, and velocity fluctuation;
- the age of air.

The experimental data include error analysis for the measuring equipment. The data are available on-line.

A CFD program with the RNG k-ε model of turbulence has been used to predict the airflow pattern, the distributions of the air temperature, concentration of tracer gas, air velocity and velocity fluctuation, and the age of air in the small office. The computed air temperature and velocity agree well with the measured data. However, some discrepancies are found between the computed and measured tracer-gas concentration in the upper part of the office. The agreement is less satisfactory between the computed and measured distribution of velocity fluctuation. The discrepancies between computed and measured age of air are 10%. Despite the discrepancies, the CFD program can be used for simulation of airflow in a room with displacement ventilation.

ACKNOWLEDGMENTS

The research is supported by MIT Cabot Solar Energy and Toda Funds, ASHRAE, National Science Foundation, Halton Group, Krueger, TROX, and Landis & Staefa, Inc.

TABLE 4
Comparison of the Age of Air Between CFD Computation and Measurement

Point	Position			The Mean Age of Air	
	x [ft (m)]	y [ft (m)]	z [ft (m)]	CFD [s]	Data [s]
1	5.8 (1.74)	6.3 (1.88)	0.5 (0.15)	575	511
2	5.8 (1.74)	6.3 (1.88)	2.2 (0.65)	728	609
3	5.8 (1.74)	6.3 (1.88)	5.2 (1.55)	1083	900
4	12.2 (3.66)	6.3 (1.88)	0.5 (0.15)	600	556
5	12.2 (3.66)	6.3 (1.88)	2.2 (0.65)	683	621
6	12.2 (3.66)	6.3 (1.88)	5.2 (1.55)	1166	888
7	8.6 (2.58)	6.3 (1.88)	8 (2.43)	1087	966

REFERENCES

Cheesewright, R., K.J. King, and S. Ziai. 1986. Experimental data for validation of computer codes for prediction of two-dimensional buoyant cavity flows. In *Significant Questions in Buoyancy Affected Enclosure or Cavity Flows*, J.A.C. Humphrey, C.T. Adedisian, and B.W. le Tourneau, eds., pp. 75-81. American Society of Mechanical Engineers.

Chen, Q., C.A. Meyers, and J. van der Kooi. 1989. Convective heat transfer in rooms with mixed convection. *Proceedings of International Seminar on Air Flow Patterns in Ventilated Spaces, University of Liege, Belgium*, pp. 69-82.

Chen, Q. 1995. Comparison of different k-ε models for indoor airflow computations. *Numerical Heat Transfer, Part B*, 28: 353-369.

Chen, Q. 1996. Prediction of room air motion by Reynolds-stress models. *Building and Environment*, 31(3): 233-244.

Launder, B.E., and D.B. Spalding. 1974. The numerical computation of turbulent flows. *Computer Methods in Applied Mechanics and Energy*, 3: 268-289.

Nielsen, P.V., A. Restivo, and J.H. Whitelaw. 1978. The velocity characteristics of ventilated rooms. *J. of Fluid Engineering*, 100: 291-298.

Yakhot, V., S.A. Orzag, S. Thangam, T.B. Gatski, and C.G. Speziale. 1992. Development of turbulence models for shear flows by a double expansion technique. *Phys. Fluids A*, 4(7): 1510-1520.

Xu, W. 1998. New turbulence models for indoor airflow modeling, Ph.D. thesis, Massachusetts Institute of Technology, Cambridge.